THE JOURNAL OF PHYSICAL CHEMISTRY C

Article

pubs.acs.org/JPCC

Ethanol Synthesis from Syngas on the Stepped Rh(211) Surface: Effect of Surface Structure and Composition

Jiancheng Wang, Zhixue Liu, Riguang Zhang,* and Baojun Wang

Key Laboratory of Coal Science and Technology of Ministry of Education and Shanxi Province, Taiyuan University of Technology, Taiyuan 030024, Shanxi, P.R. China

ABSTRACT: The mechanisms of ethanol synthesis from syngas including CH_x (x = 1−3) species and C_2 oxygenates on the stepped Rh(211) surface have been systematically investigated by using density functional theory together with a periodic slab model. Our results show that among all CH_x (x = 1−3) species, CH_3 is the most favorable monomer, which is more favorable than CH_3OH formation; this result is quite different from that on the flat Rh(111). Beginning with CH_3 species, CH_3 + CHO → CH_3CHO dominantly contributes to the formation of C_2 oxygenates; subsequently, CH_3CHO is successively hydrogenated to ethanol via CH_3CH_2O intermediate. Meanwhile, CH_4 formation by CH_3 hydrogenation is energetically compatible with CH_3CHO formation; that is, the productivity and selectivity of ethanol is determined by the formations of CH_3CHO and CH_4. As a result, the strategy of improving the Rh-based catalyst with the help from the promoter Mn is employed to tune the relative activity of CH_3CHO and CH_4 formations that control the productivity and selectivity of ethanol from syngas. Our results show that the productivity and selectivity of ethanol from syngas can be improved by introducing promoter Mn into the Rh catalyst.

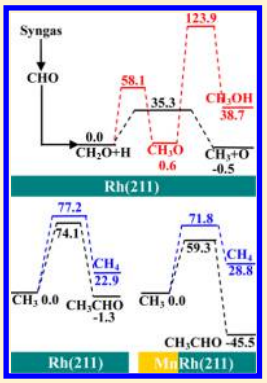

1. INTRODUCTION

Ethanol is a versatile feedstock applied in the synthesis of various products (e.g., chemicals, fuels, and polymers), and has also been used commercially as an additive or a potential substitute for gasoline.[1,2] Ethanol production from syngas is one of the major processes in industry;[3] however, one of the major hurdles for this catalytic process is low yield and poor selectivity of ethanol because of slow kinetics of the formations of CH_x and C_2 oxygenate intermediates.[3,4] Currently, Rh-based catalysts have been found to exhibit excellent catalytic performances for ethanol formation from syngas,[1,5−15] in which the catalytic performances of Rh-based catalysts are closely related to the corresponding surface structure and composition.[16,17]

For the effect of surface structure on catalytic performance, it has been long believed that under realistic conditions the important properties of most metal surfaces, including surface reactivity, are closely related to the presence of surface defects;[18−24] the surface defect plays an important role in determining reaction route and affecting the reaction activity and selectivity.[17,25,26] In fact, the step site is the most common defect for metal catalysts, which may play a key role in catalysis; previous studies have proven that the catalytic properties of metal catalysts are sensitive to surface structure, for example, González et al.[27] have reported that compared to that on the flat Rh(111) surface, NO dissociation on the stepped Rh(221) surface not only forms new adsorption sites for NO adsorption but also results in the appearance of a completely new reaction pathway; Catapan et al.[28] have investigated the water−gas shift reaction on the Ni(111) and Ni(211) surfaces, indicating that the generation of formate is favored on the stepped Ni(211); Behrens et al.[29] have revealed that methanol formation via the hydrogenation of CO and CO_2 on the stepped Cu(211) surface is more active than that on the flat Cu(111) surface; and Mavrikakis et al.[19] have shown that the activation barrier of CO dissociation on the stepped Rh(211) surface is 120 kJ mol^{-1} lower than that on the flat Rh(111) surface.

For the effect of surface composition on catalytic performance, a second metal (M), like Mn,[5,30−35] Cu,[27,36] Fe,[11,37] V,[38] or Sm,[39] is introduced into Rh to form a MRh alloy catalyst, which combines the advantage of each of its constituents because of the cooperative effect of Rh and M. As a result, the MRh alloy catalyst exhibits higher catalytic activity and selectivity, making the catalyst more efficient. For example, Li et al.[34] have examined the catalytic performance of pure and Mn-modified Rh(100) surfaces for ethanol formation from syngas, indicating that the activation barrier of CO dissociation on MnRh(100) is remarkably lowered compared to that on Rh(100). Moreover, CO insertion into CH_3 on MnRh(100) is easier than CH_4 formation by CH_3 hydrogenation; that is, the role of Mn promoter can improve the selectivity of Rh to convert syngas to ethanol. Zhao et al.[36] have shown that the production rate of C_2 oxygenates is higher than CH_4 on the RhCu(111) surface under experimental conditions, compared to that of the Rh(111) surface that is highly selective to CH_4. Recently, Choi and Liu[4] have systematically investigated ethanol formation from syngas on the flat Rh(111); their work suggested that the selectivity to ethanol from syngas largely depends on the activation barriers of CH_4 formation by CH_3 hydrogenation and C_2 oxygenate formation by CO insertion into CH_3 species and provided that introducing the promoter Fe into Rh(111) surface can suppress CH_4 formation.

Received: September 2, 2014
Published: September 8, 2014

dx.doi.org/10.1021/jp508885w | J. Phys. Chem. C 2014, 118, 22691−22701

Up to now, to the best of our knowledge, previous studies of ethanol synthesis from syngas on the Rh catalyst mainly focused on the Rh(111) and Rh(100) surfaces. Although step is the most common defect for the nanosized metal catalyst used in reality, many studies in this area are still limited.[17] Kapur et al.[25] have investigated C_1 and C_2 oxygenate formation by CO hydrogenation on the stepped Rh(211) surface by using density functional theory (DFT) calculations; however, the actual mechanism of ethanol formation from syngas on the stepped surface is still unclear. Many questions remain unanswered: (1) What are the most favored CH_x monomer and C_2 oxygenates of ethanol precursor? (2) What is the most favorable reaction pathway for ethanol formation? (3) What is the key step for controlling the productivity and selectivity of ethanol? (4) How does the stepped surface influence the catalytic performance compared to that of the flat Rh(111) surface? (5) What method can be carried out to improve the catalytic performance of the Rh catalyst?

In order to tackle these puzzles, in this study, the mechanisms of ethanol formation from syngas on the stepped Rh(211) surface have been systematically investigated by using DFT calculations. Rh(211) surface, as a defect surface, has the (100)-type step, which is generally quite active in catalytic reactions.[17,23,40] By probing into the whole reaction network, we can obtain a clear picture of ethanol formation from syngas on the stepped Rh(211) surface, and the results can provide useful information for the rational design of better Rh-based catalysts.

2. COMPUTATIONAL DETAILS

2.1. Surface Model. The stepped Rh(211) surface is modeled using a $p(2 \times 3)$ unit cell slab with eight atomic layers, and a 10 Å vacuum space is used to ensure the negligible interaction between any two successive slabs. During the calculations, the atomic positions of the upper five layers together with the adsorbed species are relaxed, whereas the bottom three layers are kept fixed at the bulk positions. According to surface morphology of Rh(211)-(2 × 3), as shown in Figure 1, nine possible adsorption sites exist on the stepped Rh(211) with the (111) terrace and (100) step. They are step edge (atop, bridge, fcc, and hcp), lower edge (fcc and hcp), terrace (atop and bridge), and (100) step (hollow site).

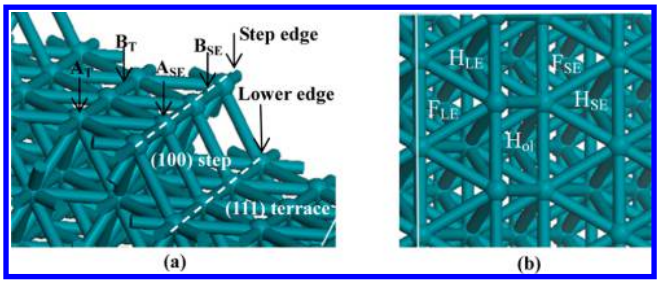

Figure 1. (a) Side view and (b) top view of Rh(211) surface morphology. A_{SE}, B_{SE}, F_{SE}, and H_{SE} refer to atop, bridge, fcc, and hcp sites on the step edge (SE), respectively. F_{LE} and H_{LE} refer to fcc and hcp sites on the lower edge (LE), respectively. A_T and B_T refer to atop and bridge sites on the (111) terrace, respectively, and Hol refers to the hollow sites on the stepped surface.

2.2. Calculation Methods. The Vienna Ab Initio Simulation Package (VASP),[41−43] implementing the DFT with a three-dimensional (3D) periodic boundary condition, has been employed for all calculations. The generalized gradient approximation (GGA) with Perdew−Wang formulation (PW91) is used for the exchange-correlation function.[44] The electron−ion interaction is modeled by the projected-augmented wave (PAW) method.[45] The Brillouin zone is sampled using a 4 × 4 × 1 Monkhorst−Pack *k*-point grid[46] with the Methfessel−Paxton smearing of 0.1 eV.[47] The plane-wave cutoff energy is set at 400 eV to describe the electronic wave functions. A force difference between two steps less than 0.01 eV Å^{-1} is used as the criterion for convergence of ionic relaxation. The relaxation of the electronic degrees of freedom is assumed to be converged if the total energy change and the band structure energy change between two steps are both smaller than 5 × 10^{-6} eV.

Reaction pathways have been investigated using the climbing-image nudged elastic band method (CI-NEB).[48,49] Transition states have been optimized using the dimer method.[50,51] The structure of a transition state is deemed converged when the forces acting on the atoms were all <0.05 eV Å^{-1} for the various degrees of freedom set in the calculation. The molecules in the gas phase are calculated using a 10 × 10 × 10 Å^3 cubic unit cell.

3. RESULTS AND DISCUSSION

In this section, the adsorptions of reactants and all possible intermediates are first investigated on the stepped Rh(211) surface; then, the formation mechanisms of CH_x (x = 1−3) species, C_2 oxygenates, and ethanol are discussed on the stepped Rh(211). The differences of ethanol formation between the stepped Rh(211) and the flat Rh(111) surfaces are then identified to obtain the effect of surface structures on reaction mechanism of ethanol formation; finally, an expanded strategy of improved catalytic performance of an Rh-based catalyst by introducing a promoter metal to change surface composition has been proposed.

3.1. Adsorption of All Possible Species in Ethanol Synthesis. For the adsorption of various reactants, intermediates, and products on the stepped Rh(211) surface, the adsorption energy is defined as $E_{ads} = E_{Rh(211)} + E_{adsorbate} - E_{adsorbate/Rh(211)}$, where the $E_{adsorbate/Rh(211)}$ is the total energy of Rh(211) slab with the adsorbate, $E_{Rh(211)}$ the energy of clean Rh(211) surface and $E_{adsorbate}$ the energy of gas-phase adsorbate. Herein, spin-polarized calculations are carried out for the gas-phase radical species involved in ethanol formation from syngas. By this definition, a negative value corresponds to exothermic adsorption.

As the starting point, the adsorption of various reactants, intermediates, and products is investigated on the stepped Rh(211), in which nine possible adsorption sites are considered. Only the most stable configurations of these species obtained by our calculations are shown in Figure 2. Table 1 summarizes the adsorption site, the corresponding adsorption energy, and the important geometric parameters of these stable configurations.

Our results show that the majority of the stable configurations for C_1 and C_2 oxygenates are adsorbed at the step edge sites, except for COH bonding to the hollow site via C atom. Our results are consistent with the available literature data from previous studies.[17,25] On the other hand, when compared to the adsorption sites and adsorption energies on the flat Rh(111) surface,[4,25] our results on the stepped Rh(211) surface show that the different surface structures not only result in different adsorption sites of adsorbed species but also lead to

dx.doi.org/10.1021/jp508885w | J. Phys. Chem. C 2014, 118, 22691−22701

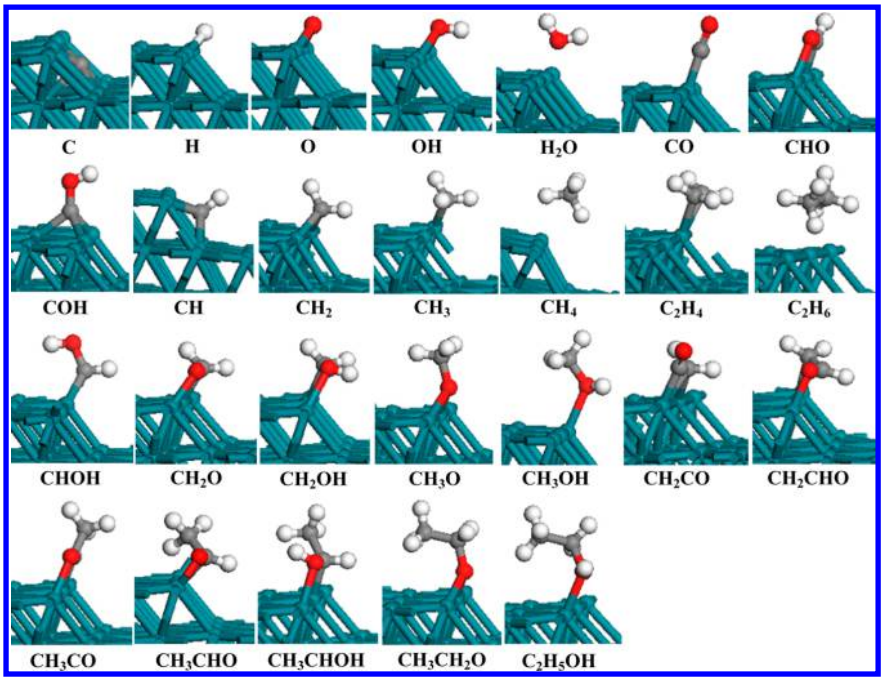

Figure 2. Most stable configuration of possible species involved in ethanol formation from syngas. C, O, H, and Rh atoms are shown in gray, red, white, and dark cyan, respectively.

different adsorption strength. Compared to the surface atom on the flat Rh(111) surface, Zhang et al.[17] have shown that the lower coordination number of step metal atoms on the stepped Rh(211) surface mainly contributes to the high adsorption strength of adsorbed species, in which the extra dangling bonds induced by the defect make the surface step more active in catalytic reactions.

3.2. CH_x (x = 1−3) Formation. Starting from the adsorbed CO species, two possibilities exist for the formation of CH_x (x = 1−3) species; one is the direct C−O bond scission of CO to C and O atoms followed by C hydrogenation to CH_x (x = 1−3) species, and the other is CO hydrogenation to CH_xO oxygenates followed by its C−O bond scission to form CH_x (x = 1−3) species in the presence or absence of hydrogen. First, we investigate CO dissociation and hydrogenation. As shown in Table 2, three reactions (R1−R3) may occur.

Figure 3 presents the relative energy profile of these reactions together with the structures of initial states (ISs), transition states (TSs), and final states (FSs). It can be seen that the activation barriers of COH and CHO formation are 196.3 and 121.9 kJ mol^{-1}, respectively, which are more favorable than direct CO dissociation. CHO formation is more preferred. Therefore, the adsorbed CO species on the stepped Rh(211) is dominantly hydrogenated to form CHO (R2); similarly, Choi and Liu[4] have shown that CHO species exist in the reaction of CO hydrogenation on the flat Rh(111). Furthermore, previous experiments using the chemical trapping approach proposed the significance of CHO species for alcohol synthesis on Rh/SiO_2 catalysts.[52]

3.2.1. CH Formation. Above results show that CHO is the dominant product for the adsorbed CO species on the stepped Rh(211); thus, starting from the initial state CHO and CHO + H, four possible pathways with five elementary reactions (R4−R8) are responsible for CH formation, as shown in Table 2. Meanwhile, CHO hydrogenation to CH_2O (R9) is also considered. Figure 4 provides the relative energy profiles of these reactions together with the structures of ISs, TSs, and FSs.

As illustrated in Figure 4, starting with CHO or CHO + H, among the four reaction pathways of CH formation, the pathway of CHO + H → CHOH → CH + OH (R6, R7) is dominantly responsible for CH formation via CHOH intermediate, which has the highest barrier of 134.9 kJ mol^{-1} with the reaction energy of −36.4 kJ mol^{-1}. However, the pathway of CHO + H → CH_2O (R9) has the highest barrier and reaction energy of 68.6 and 46.5 kJ mol^{-1}, respectively. These results demonstrate that CH_2O is the dominant product by CHO hydrogenation rather than CH species by direct CHOH dissociation.

3.2.2. CH_2 Formation. As mentioned above, CH_2O is preferred to be formed by CHO hydrogenation. Thus, starting from CH_2O and CH_2O + H, as listed in Table 2, four possible pathways with five elementary reactions (R11−R15) are responsible for CH_2 formation; meanwhile, CH_3O formation by CH_2O hydrogenation to (R16) is also considered. In addition, H-assisted CHO dissociation can also produce CH_2 species (R10). The relative energy profile of these reactions together with the structures of ISs, TSs, and FSs are presented in Figure 5.

As presented in Figure 5, starting with CH_2O or CH_2O + H, among five reaction pathways of CH_2 formation, the pathway of CHO + 2H → CH_2O + H → CH_2 + OH (R9, R12) is dominantly responsible for CH_2 formation, which has the highest barrier of 127.9 kJ mol^{-1} with the reaction energy of −0.6 kJ mol^{-1}. However, the pathway of CH_2O + H → CH_3O (R16) has the highest barrier and reaction energy of 104.6 and 47.1 kJ mol^{-1}, respectively. These results demonstrate that CH_3O rather than CH_2 species is the dominant product of CH_2O hydrogenation.

3.2.3. CH_3 Formation. As mentioned above, CH_2O hydrogenation prefers to form CH_3O; thus, we further investigate CH_3 formation, starting from CH_3O and CH_3O + H. H-assisted CH_2O dissociation can also produce CH_3 species

dx.doi.org/10.1021/jp508885w | J. Phys. Chem. C 2014, 118, 22691−22701

Table 1. Adsorption Energies and Key Geometrical Parameters of All Possible Species Involved in Ethanol Formation from Syngas on the Stepped Rh(211) Surface

species	E_{ads} (kJ mol^{-1})	configuration	d_{Rh-C} (Å)	d_{Rh-O} (Å)
C	760.4	hollow	1.984, 1.984, 2.001, 2.001	
H	272.3	bridge-SE	Rh−H: 1.770, 1.770	
O	547.4	bridge-SE		1.899, 1.899
OH	369.1	bridge-SE via O		2.097, 2.097
H_2O	47.4	away from surface		
CO	201.4	atop-SE via C	1.857	
CHO	283.7	bridge-SE via C and O	1.935	2.146
COH	452.9	hcp-SE via C	1.995, 2.007, 2.011	
CH	674.9	hollow	2.105, 2.106, 2.107, 2.107	
CH_2	430.6	bridge-SE via C	2.024, 2.024	
CH_3	229.3	atop-SE via C	2.111	
CH_4	15.1	away from surface	2.602	
C_2H_4	125.7	atop-SE via C1 and C2	2.134, 2.128	
C_2H_6	22.2	away from surface	2.743, 2.940	
CHOH	341.2	bridge-SE via C	2.051, 2.052	
CH_2O	122.6	bridge-SE via C and O	2.101	1.992
CH_2OH	231.4	bridge-SE via C and O	2.058	2.231
CH_3O	281.8	bridge-SE via O		2.090, 2.091
CH_3OH	63.9	atop-SE via O		2.225
CH_2CO	163.0	bridge-SE via α-C and β-C	α: 2.240, 2.244; β: 1.937	
CH_2CHO	282.8	bridge-SE via β-C and O	2.161	2.028
CH_3CO	276.5	bridge-SE via α-C and O	1.957	2.134
CH_3CHO	99.3	bridge-SE via α-C and O	2.186	2.021
CH_3CHOH	221.5	bridge-SE via α-C and O	2.076	2.219
CH_3CH_2O	279.9	bridge-SE via O		2.089, 2.088
C_2H_5OH	63.4	atop-SE via O		2.222

(R17). In addition, CH_3O hydrogenation to CH_3OH (R20) is also considered. The corresponding potential energy diagram for these processes together with the structures of ISs, TSs, and FSs are shown in Figure 6.

We can obtain from Figure 6 that the pathway of CHO + 2H → CH_2O + H → CH_3 + O is the most favorable pathway for CH_3 formation, which has the highest barrier of 81.8 kJ mol^{-1}; the rate-controlling step (R9) has the activation barrier of 68.6 kJ mol^{-1}. Meanwhile, CH_3OH formation has the highest barrier of 170.4 kJ mol^{-1}; the rate-controlling step (R20) has the activation barrier of 123.3 kJ mol^{-1}. More importantly, starting with CH_2O + H, the reaction of CH_2O + H → CH_3 + O (R17) with the activation barrier of 35.3 kJ mol^{-1} is more favorable than the reaction of CH_2O + H → CH_3O (R16); thus, the CH_3 species is the dominant product by hydrogen-assisted CH_2O dissociation rather than CH_3O by CH_2O hydrogenation, as well as CH_3OH by CH_3O hydrogenation.

3.2.4. Brief Summary about CH_x (x = 1−3) and CH_3OH Formation. With respect to CHO + H, Figure 7 presents the potential energy profile for the most favorable pathway of CH_x (x = 1−3) species and CH_3OH formations. CH formation (black line) has the highest barrier of 134.9 kJ mol^{-1}; CH_2 formation (red line) has the highest barrier of 127.9 kJ mol^{-1}; CH_3 formation (blue line) has the highest barrier of 81.8 kJ mol^{-1}. CH_3OH formation (green line) has the highest barrier of 170.4 kJ mol^{-1}. The above results show that among all CH_x (x = 1−3) species, CH_3 is the most favorable monomer via the reaction process of CO + 3H → CHO + 2H → CH_2O + H → CH_3 + O (R2, R9, R17). CH_3 formation is energetically more favorable than CH_3OH formation. Our results on the stepped Rh(211) are quite different from those obtained on the flat Rh(111).[4] Thus, the stepped Rh(211) surface can catalyze the conversion reaction of syngas to form the important intermediate CH_3 with high selectivity rather than forming CH_3OH.

3.3. Formation of C_2 Oxygenates and Ethanol. For C_2 oxygenate formation, Zhao et al.[53] have shown that CHO insertion into CH_x (x = 1−3) is superior or competitive to CO insertion; thus, CO/CHO insertion into CH_3 to C_2 oxygenates has been considered. Meanwhile, CH_3 species will undergo the reaction of hydrogenation, dissociation, and coupling. Figure 8 presents the potential energy profile of these reactions related to CH_3 species together with the structures of ISs, TSs, and FSs.

As shown in Figure 8, among all reactions related to CH_3 species, CH_3 coupling (R25) and CO insertion into CH_3 (R21) are more difficult to realize because of the high activation barrier, whereas CH_3 dissociation into CH_2 and H (R24) is the most favorable with activation barrier and reaction energy of 48.5 and 5.6 kJ mol^{-1}, respectively. The second is CHO insertion into CH_3 to CH_3CHO (R22). This elementary reaction has an activation barrier and reaction energy of 74.1 and −1.3 kJ mol^{-1}, respectively. The third is CH_3 hydrogenation to CH_4 (R23). This elementary reaction has an activation barrier and reaction energy of 77.2 and 22.9 kJ mol^{-1}, respectively.

As mentioned above, because of easy formation of CH_2 by CH_3 dissociation, we further investigate the hydrogenation, dissociation, and coupling of CH_2 (R28−R30), as well as CO/CHO insertion into CH_2 (R26, R27), as shown in Figure 9. Our results show that CH_2 prefers to be hydrogenated to CH_3; thus, once the CH_2 species is formed, among all reactions related to the CH_2 species, CH_3 is the dominant product. On the other hand, the above results also show that CHO insertion into CH_2 and CH_3 are responsible for the formation of C_2 oxygenates; thus, starting from the CH_3 species, C_2 oxygenate formation via CH_3 + CHO → CH_2 + CHO → CH_2CHO (R24, R27) has the highest barrier of 67.4 kJ mol^{-1}, which is energetically compatible with the reaction of CH_3 + CHO → CH_3CHO (R22) with the activation barrier of 74.1 kJ mol^{-1}. Furthermore, CH_2CHO undergoes hydrogenation to ethanol. However, it is noted that when CHO insertion into CH_2 occurs, most of the CH_2 species mainly participate in hydrogenation to CH_3; that is, a small quantity of CH_2 species is involved in CHO insertion to CH_2CHO, suggesting that C_2 oxygenate formation mainly depends on the CHO insertion into CH_3 to CH_3CHO.

dx.doi.org/10.1021/jp508885w | J. Phys. Chem. C 2014, 118, 22691−22701

Table 2. Possible Elementary Reactions Involved in Ethanol Synthesis from Syngas Together with the Activation Energies (E_a) and Reaction Energies (ΔH)

	elementary reactions	transition state	E_a(kJ mol^{-1})	ΔH (kJ mol^{-1})
R1	CO → C + O	TS1	396.3	64.5
R2	CO + H → CHO	TS2	121.9	85.0
R3	CO + H → COH	TS3	196.3	95.5
R4	CHO → CH + O	TS4	251.4	0.6
R5	CHO + H → CH + OH	TS5	152.8	−36.4
R6	CHO + H → CHOH	TS6	120.9	31.4
R7	CHOH → CH + OH	TS7	103.5	−67.8
R8	CHOH + H → CH + H_2O	TS8	179.2	−5.7
R9	CHO + H → CH_2O	TS9	68.6	46.5
R10	CHO + H → CH_2 + O	TS10	205.9	44.0
R11	CH_2O → CH_2 + O	TS11	159.4	−2.5
R12	CH_2O + H → CH_2 + OH	TS12	81.4	−47.1
R13	CH_2O + H → CH_2OH	TS13	101.4	−3.3
R14	CH_2OH → CH_2 + OH	TS14	83.9	−43.8
R15	CH_2OH + H → CH_2 + H_2O	TS15	94.0	−25.1
R16	CH_2O + H → CH_3O	TS16	58.1	0.6
R17	CH_2O + H → CH_3 + O	TS17	35.3	−0.5
R18	CH_3O → CH_3 + O	TS18	175.3	−1.1
R19	CH_3O + H → CH_3 + OH	TS19	153.7	−30.0
R20	CH_3O + H → CH_3OH	TS20	123.3	38.1
R21	CH_3 + CO → CH_3CO	TS21	141.8	44.9
R22	CH_3 + CHO → CH_3CHO	TS22	74.1	−1.3
R23	CH_3 + H → CH_4	TS23	77.2	22.9
R24	CH_3 → CH_2 + H	TS24	48.5	5.6
R25	CH_3 + CH_3 → C_2H_6	TS25	220.8	−10.4
R26	CH_2 + CO → CH_2CO	TS26	85.7	66.0
R27	CH_2 + CHO → CH_2CHO	TS27	61.8	−51.6
R28	CH_2 + H → CH_3	TS28	42.9	−5.6
R29	CH_2 → CH + H	TS29	56.6	−42.8
R30	CH_2 + CH_2 → C_2H_4	TS30	68.7	−47.6
R31	CH_3CHO + H → CH_3CH_2O	TS31	51.5	−0.9
R32	CH_3CHO + H → CH_3CHOH	TS32	101.8	−1.7
R33	CH_3CH_2O + H → C_2H_5OH	TS33	131.1	38.4

Thus, starting from the dominant CH_3 species, CHO insertion into CH_3 to CH_3CHO is the most favorable pathway leading to the formation of C_2 oxygenates. Meanwhile, beginning with CHO species, CHO hydrogenation to CH_2O has an activation barrier and reaction energy of 68.6 and 46.5 kJ mol^{-1}, respectively, which are energetically compatible with CHO insertion into CH_3 to CH_3CHO; thus, when CHO insertion into CH_3 occurs, partial CHO can also participate in hydrogenation to CH_2O, and the rest is involved in insertion to CH_3CHO. On the other hand, for the formation of C_2 oxygenates, CO insertion into CH_3 has an activation barrier higher than that of CHO insertion, and CO hydrogenation to CHO has an activation barrier of 121.9 kJ mol^{-1}, which is lower than CO insertion into CH_3 with the activation barrier of 141.8 kJ mol^{-1}. As a result, CO prefers to be hydrogenated to CHO rather than CO insertion into CH_3 to CH_3CO, suggesting that C_2 oxygenates are dominantly formed by CHO insertion into CH_3 rather than CO insertion into CH_3.

Furthermore, one can see that for the dominant CH_3 species, CH_4 formation by CH_3 hydrogenation and CH_3CHO formation by CHO insertion into CH_3 can energetically compete because of the very small difference of the activation barrier by 3.1 kJ mol^{-1}, suggesting that on the stepped Rh(211) CH_3CHO formation is energetically compatible with CH_4 formation, which reduces the productivity and selectivity of ethanol from syngas.

Finally, starting from CH_3CHO species, there are two possibilities for CH_3CHO hydrogenation, as seen in Figure 10. One is the formation of CH_3CH_2O by adding H to the α-C atom (R31), which needs to overcome an activation barrier of 51.5 kJ mol^{-1} with the reaction energy of −0.9 kJ mol^{-1}. The other is the formation of CH_3CHOH by adding H to the O

dx.doi.org/10.1021/jp508885w | J. Phys. Chem. C 2014, 118, 22691−22701

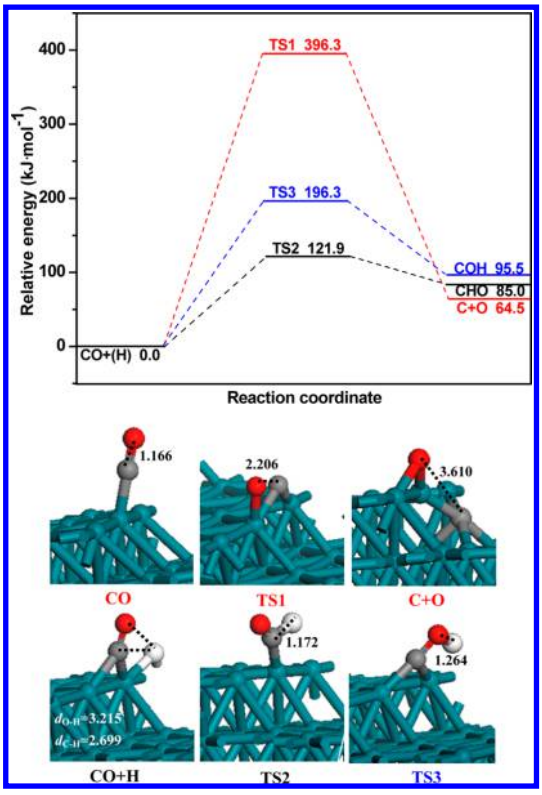

Figure 3. Potential energy diagram of CO initial step together with the initial states, transition states, and final states. Bond lengths are in angstroms. See Figure 2 for color coding.

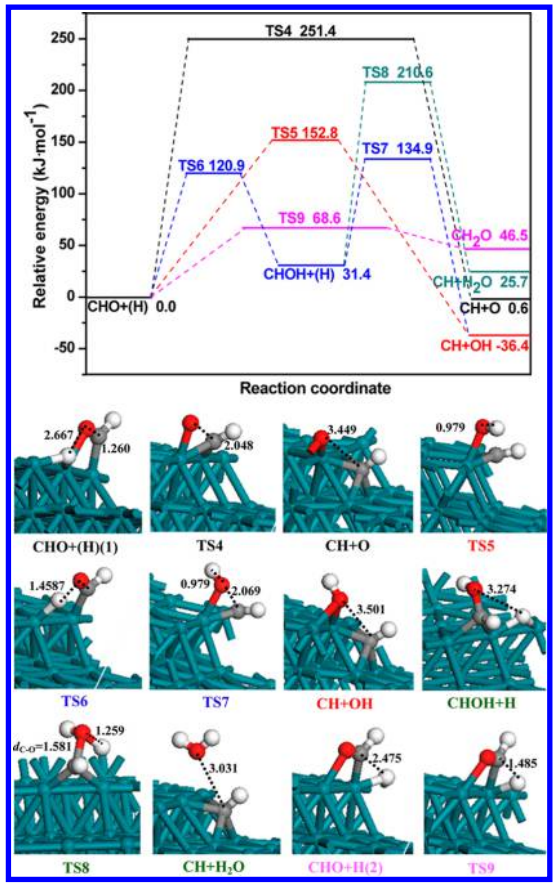

Figure 4. Potential energy diagram of CH and CH_2O formations together with initial states, transition states, and final states. Bond lengths are in angstroms. See Figure 2 for color coding.

atom (R32). This elementary reaction has an activation barrier of 101.8 kJ mol^{-1}, which is higher by 50.3 kJ mol^{-1} than that of CH_3CH_2O formation; thus, CH_3CHO prefers to be hydrogenated to CH_3CH_2O rather than forming CH_3CHOH, in which CH_3CHO desorption cannot compete with CH_3CHO hydrogenation to CH_3CH_2O. Finally, CH_3CH_2O hydrogenation can form C_2H_5OH (R33). This elementary reaction needs to overcome an activation barrier of 131.1 kJ mol^{-1} with the reaction energy of 38.4 kJ mol^{-1}.

3.4. Comparisons of C_2H_5OH Formation between Rh(211) and Rh(111) Surfaces. Previous DFT studies about ethanol formation from syngas on the flat Rh(111) have been obtained by Choi and Liu,[4] which suggest that CH_3 is the most favorable monomer among all CH_x species and that the selectivity to ethanol on Rh(111) is controlled by CH_4 formation by CH_3 hydrogenation and C_2 oxygenate formation by CO insertion into CH_3 species. Thus, it is interesting to carry out the qualitative comparisons about the key reaction steps on the flat Rh(111) by Choi and Liu with our present results on the stepped Rh(211).

3.4.1. CH_3 and CH_3OH Formation. Figure 11 presents the potential energy profile for the optimal pathway of CH_3 and CH_3OH formations on both Rh(211) and Rh(111) surfaces. We can obtain that methanol formation goes through the same favorable route of CO + 4H → CHO + 3H → CH_2O + 2H → CH_3O + H → CH_3OH. More importantly, on the Rh(111) surface, CH_3OH formation is more favorable than CH_3 formation; however, on the Rh(211) surface, CH_3 formation is more favorable than CH_3OH formation. Thus, for syngas conversion, the stepped Rh(211) surface exhibits high activity and selectivity to CH_3 species formation rather than CH_3OH. As a result, the CH_3 source is increased. Because CH_x is proposed to be a prerequisite for C_2 oxygenate formation from syngas, the stepped Rh(211) surface may boost ethanol formation compared to that of the flat Rh(111).

3.4.2. C_2 Oxygenates and CH_4 Formation. As mentioned above, among all CH_x (x = 1−3) species, CH_3 is the most favorable monomer on both Rh(211) and Rh(111) surfaces. Figure 12 presents the potential energy profile for the optimal pathway of CH_4 and C_2 oxygenate formations on both Rh(211) and Rh(111) surfaces starting from CH_3 species. The results show that on the flat Rh(111), C_2 oxygenates are dominantly formed by CO insertion into CH_3 to CH_3CO; meanwhile, CH_4 formation by CH_3 hydrogenation is much more favorable than CH_3CO, suggesting that the flat Rh(111) surface exhibits a better selectivity to hydrocarbons rather than C_2 oxygenates; however, on the stepped Rh(211), C_2 oxygenates are dominantly formed by CHO insertion into CH_3 to CH_3CHO, which is quite different from that on the flat Rh(111). CH_3CHO formation is energetically compatible with CH_4 formation by CH_3 hydrogenation because of the very small difference of activation barrier (3.1 kJ mol^{-1}), indicating that compared to that of the flat Rh(111) surface, the stepped Rh(211) surface exhibits a better selectivity to C_2 oxygenates.

On the basis of the above qualitative comparisons about the key reaction steps between the flat Rh(111) and the stepped Rh(211) surfaces, our results indicate that Rh(211) not only leads to the new formation pathway of CH_3 species and C_2 oxygenates but also boosts the formations of CH_3 species and C_2 oxygenates. As a result, the productivity and selectivity of ethanol from syngas on the stepped Rh(211) surface can be

dx.doi.org/10.1021/jp508885w | J. Phys. Chem. C 2014, 118, 22691−22701

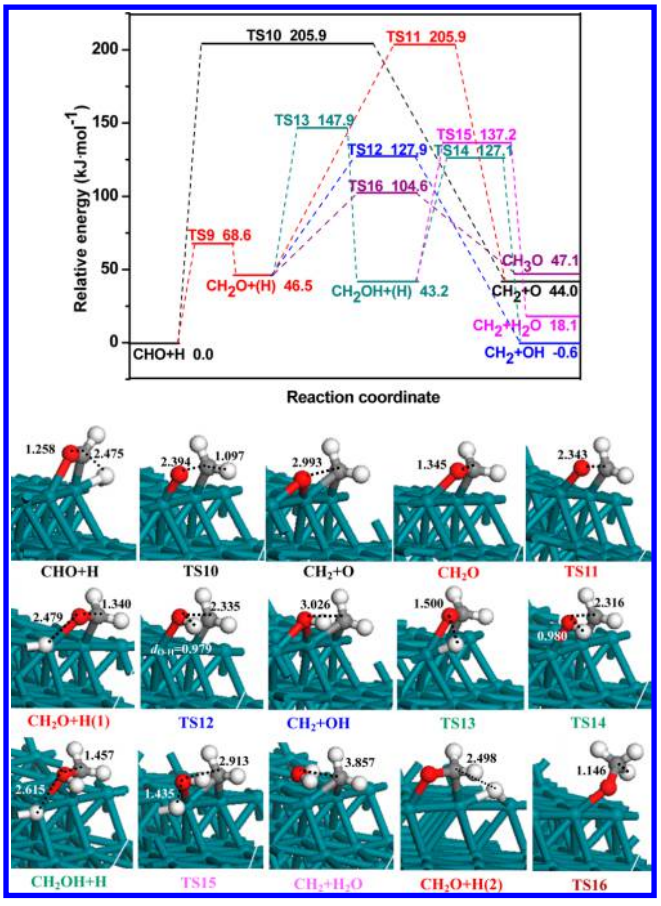

Figure 5. Potential energy diagram of CH_2 and CH_3O formations together with initial states, transition states, and final states. Bond lengths are in angstroms. See Figure 2 for color coding.

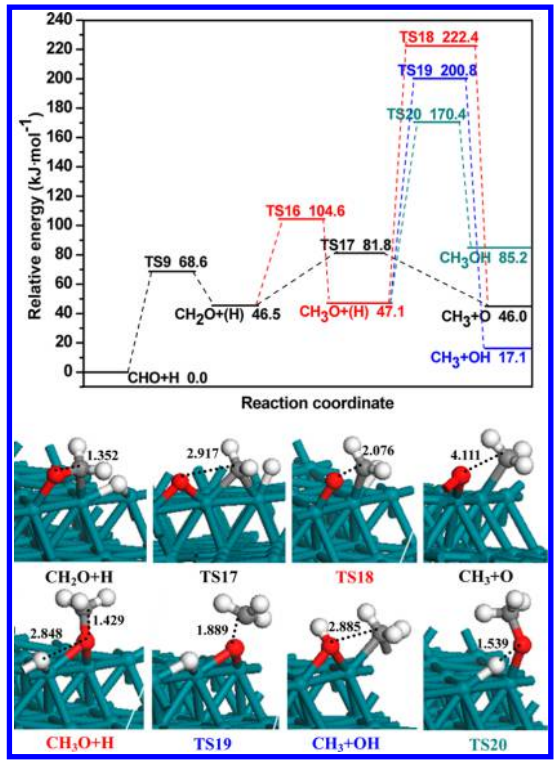

Figure 6. Potential energy diagram for CH_3 and CH_3OH formations together with initial states, transition states, and final states. Bond lengths are in angstroms. See Figure 2 for color coding.

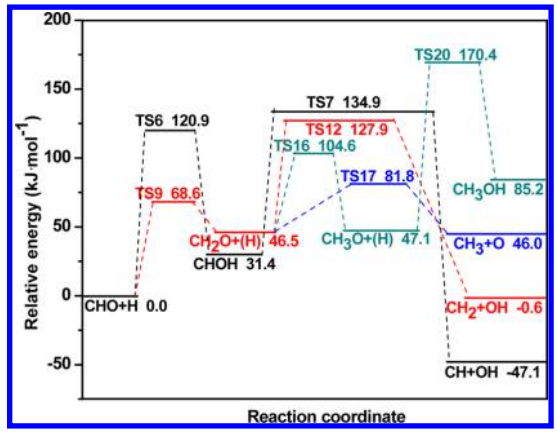

Figure 7. Potential energy diagram of the most favorable route for the formation of CH_x (x = 1−3) species and CH_3OH.

improved compared to that of the flat Rh(111) sruface. In addition, starting from C_2 oxygenates, on Rh(111), ethanol is formed via the route $CH_3CO + 3H \rightarrow CH_3COH + 2H \rightarrow CH_3CHOH + H \rightarrow C_2H_5OH$; however, on Rh(211), ethanol is formed via the route $CH_3CHO + 2H \rightarrow CH_3CH_2O + H \rightarrow C_2H_5OH$.

3.5. General Discussion. As shown in Figure 13, the optimal pathway of ethanol formation from syngas on the stepped Rh(211) first goes through the process of $CO + 3H \rightarrow CHO + 2H \rightarrow CH_2O + H \rightarrow CH_3 + O$ to produce CH_3 species, which is the most favored CH_x monomer; then, CHO insertion into CH_3 can form CH_3CHO, followed by successive hydrogenation via CH_3CH_2O intermediate to ethanol. Meanwhile, CH_3 formation is much easier than CH_3OH formation; that is, the stepped Rh(211) surface can boost CH_3 source contributing to the formation of C_2 oxygenates. However, starting from CH_3 species, CH_3CHO formation is energetically compatible with CH_4 formation, which reduces the productivity and selectivity of C_2 oxygenates. As a result, Rh(211) has relatively low selectivity for C_2H_5OH from syngas because of the easy formation of CH_4.

According to our above analysis, starting from CH_3 species, by suppressing the formation of CH_4, more CH_3 species can participate in the formation of CH_3CHO by CHO insertion into CH_3; thus, the production of C_2H_5OH increases. On the other hand, high production of C_2H_5OH can also be obtained by lowering the activation barrier of CH_3CHO formation. In this way, CH_4 formation also cannot compete with CH_3CHO; as a result, more C_2H_5OH is produced compared to CH_4. Therefore, only two variables significantly affect the productivity and selectivity of C_2H_5OH. One is the activation barrier of CH_4 formation by CH_3 hydrogenation; the other is the activation barrier of CHO insertion into CH_3. To achieve high productivity and selectivity of ethanol, the Rh catalyst has to get help from other promoters and/or supports, by which CH_4 formation should be minimized and/or C_2 oxygenate formation from C_1 oxygenates should be maximized. Up to now, previous studies have shown that the catalytic activity and/or selectivity of the Rh catalyst can be improved by introducing promoters into Rh catalysts;[8−11,54] for example, the promoter Mn can increase the activity and selectivity of C_2 oxygenate formation;[5,30−34] meanwhile, the experimental study by Luo et al. further found that the addition of Mn is essential for the

dx.doi.org/10.1021/jp508885w | J. Phys. Chem. C 2014, 118, 22691−22701

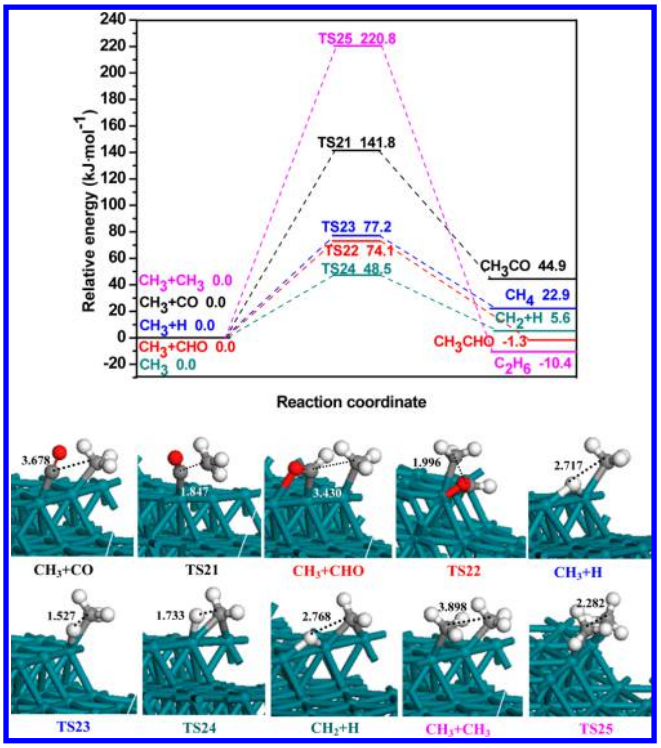

Figure 8. Potential energy diagram of the reactions related to CH_3 species together with initial states, transition states, and final states. Bond lengths are in angstroms. See Figure 2 for color coding.

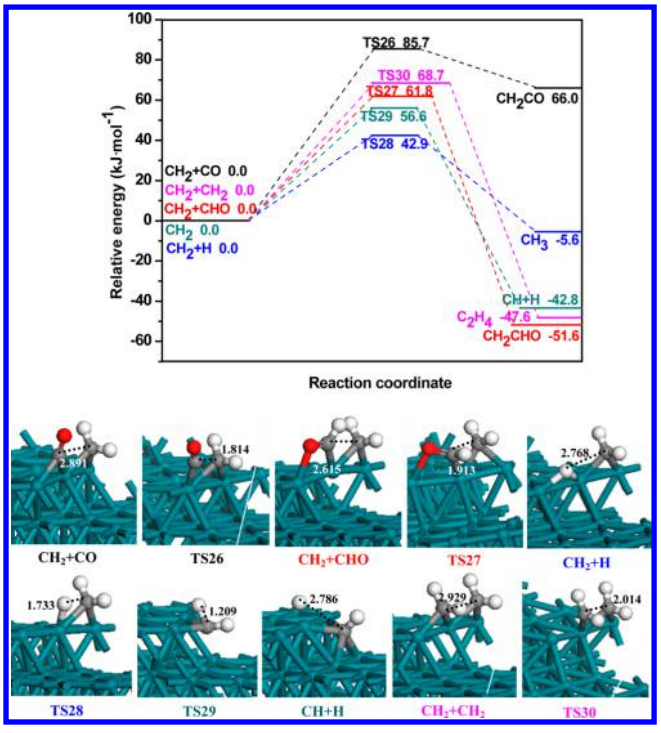

Figure 9. Potential energy diagram of the reactions related to CH_2 species together with initial states, transition states, and final states. Bond lengths are in angstroms. See Figure 2 for color coding.

formation of acetic acid and acetaldehyde with high selectivity.[55]

To validate our predictions about the role of promoter metal and further probe the effect of surface composition on catalytic performance, as mentioned above, we examined the role of

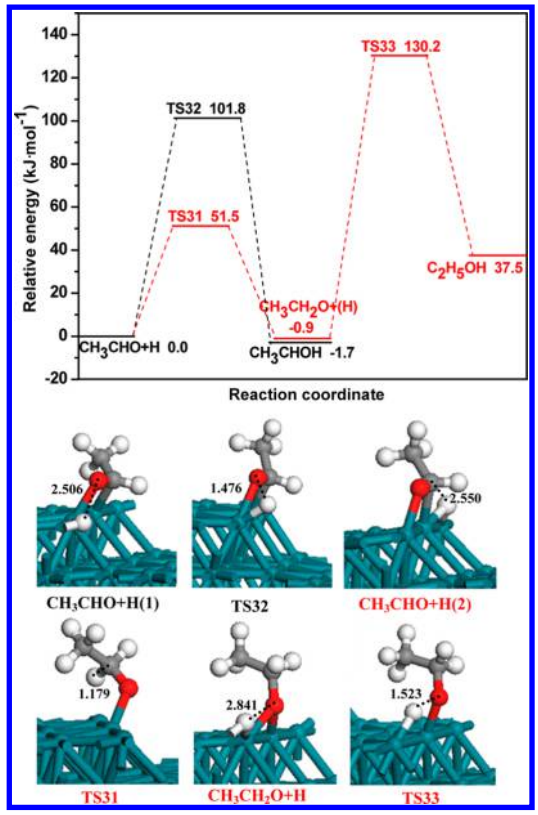

Figure 10. Potential energy diagram of CH_3CHO further hydrogenation to ethanol together with initial states, transition states, and final states. Bond lengths are in angstroms. See Figure 2 for color coding.

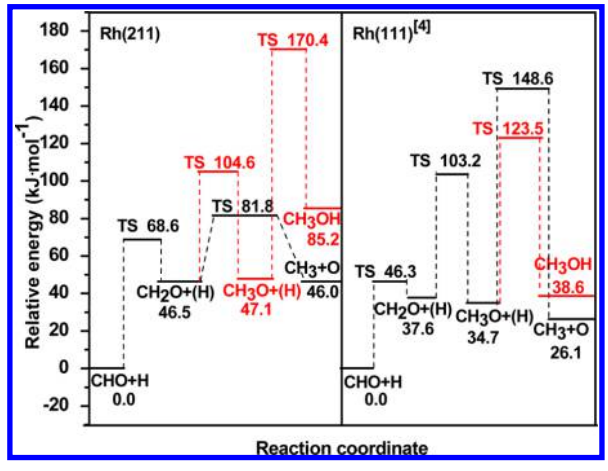

Figure 11. Potential energy profile for the optimal pathway of CH_x (x = 1−3) and CH_3OH formation from syngas on Rh(211) and Rh(111) surfaces.

promoter Mn and its effect on the catalytic activity and selectivity. For the MnRh(211) surface, two types of models exist: one replaces a Rh atom by a Mn atom, and the other adsorbs a surface Mn atom onto the Rh surface. Up to now, a large number of studies about the effect of the promoter on C_2 oxygenate formation from syngas mainly focused on the first type of model.[3,4,34,36] Thus, in our study, only the first model with a Rh atom replaced by a Mn atom is employed as the promoter Mn-doped Rh(211) model. Of course, the surface Mn adatom on the Rh surface is also important for investigating the effect of the promoter on ethanol synthesis from syngas,

dx.doi.org/10.1021/jp508885w | J. Phys. Chem. C 2014, 118, 22691−22701

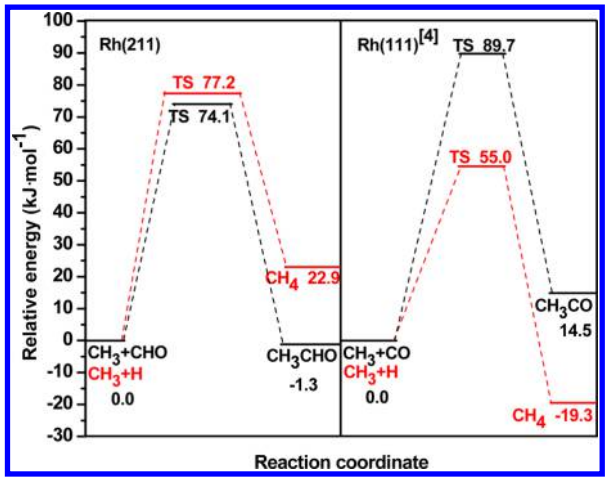

Figure 12. Comparison of potential energy diagram for C_2 oxygenates and CH_4 formation on Rh(211) and Rh(111) surfaces.

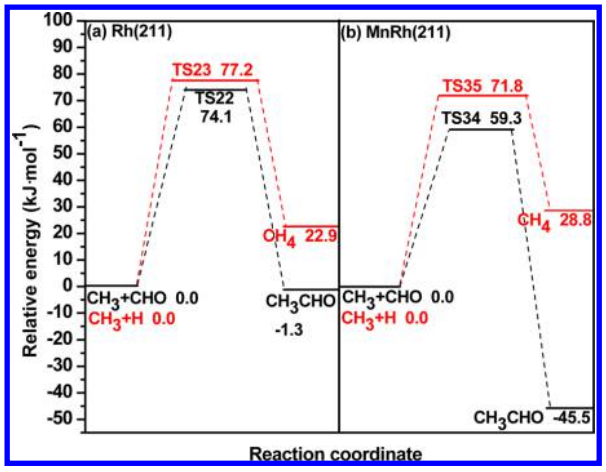

Figure 14. Comparison of potential energy diagrams for CH_3CHO and CH_4 formation on Rh(211) and MnRh(211) surfaces.

which will be carried out in our next work. For the promoter Mn-doped MnRh(211) surface, there are three choices for the Mn atom on Rh(211) surface: a step edge, a terrace, and a step base site. Our results show that the MnRh(211) surface with one Mn atom at the step edge is found to be the most easily formed.

Figure 14 presents the comparison of potential energy diagrams for CH_3CHO and CH_4 formation on Rh(211) and MnRh(211) surfaces. These results show that on the Rh(211) surface, CH_3CHO formation is energetically compatible with CH_4 formation by CH_3 hydrogenation because of the very small difference of activation barrier and reaction energy by 3.1 and 24.2 kJ mol^{-1}, respectively, indicating that the Rh(211) surface exhibits a poor selectivity to C_2 oxygenates. However, on MnRh(211), CH_3CHO formation by CHO insertion into CH_3 requires an activation barrier of 59.3 kJ mol^{-1} with the reaction energy of −45.5 kJ mol^{-1}, while CH_4 formation by CH_3 hydrogenation has an activation barrier of 71.8 kJ mol^{-1} with the reaction energy of 28.8 kJ mol^{-1}. Thus, compared to Rh(211), Mn-promoted MnRh(211) reduces the activation barrier of CH_4 and CH_3CHO formations; that is, the activity of Mn-promoted MnRh(211) increases. More importantly, CH_3CHO formation is much more favorable than CH_4 formation, both kinetically and thermodynamically, because of the relatively large difference of activation barrier and reaction energy by 12.5 and 74.3 kJ mol^{-1}, respectively, indicating that the Mn-promoted MnRh(211) surface exhibits a good selectivity to C_2 oxygenates rather than CH_4. This result

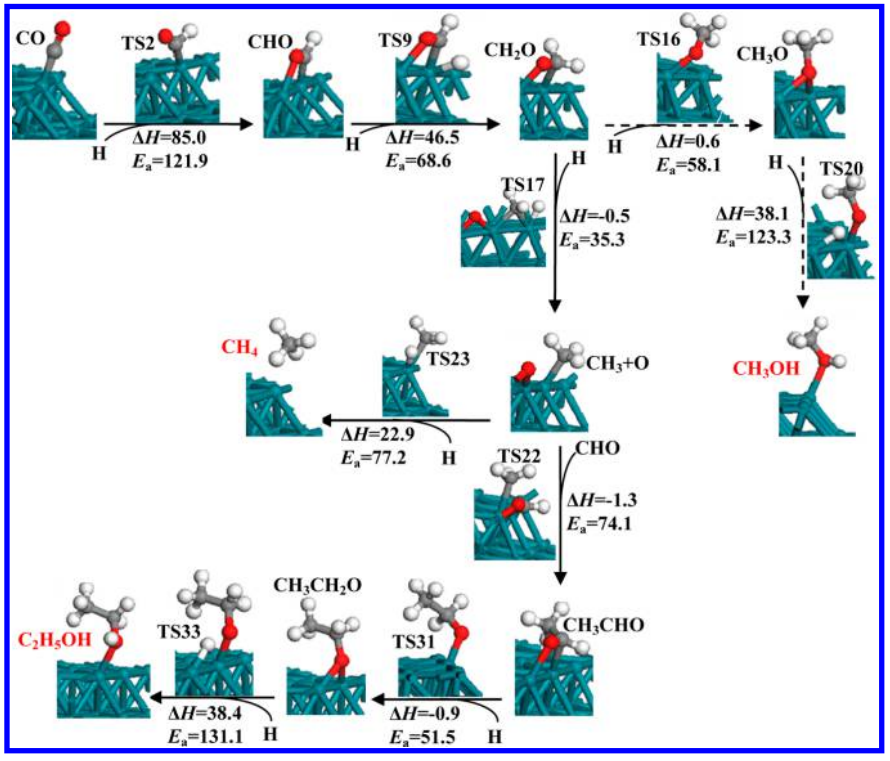

Figure 13. Optimal reaction pathway of ethanol formation from syngas on the stepped Rh(211) with the reaction energies and activation barriers of elementary reactions CH_4, CH_3OH, and C_2H_5OH formations. The data unit is kilojoules per mole. See Figure 2 for color coding.

dx.doi.org/10.1021/jp508885w | J. Phys. Chem. C 2014, 118, 22691−22701

suggests that the promoter Mn increases the activity and selectivity of C_2 oxygenate formation, which agrees well with the reported experimental results.[5,30−34]

4. CONCLUSIONS

In this study, we investigate the mechanism of ethanol synthesis from syngas on the stepped Rh(211) surface by means of density functional theory method together with a periodic slab model. In addition, the differences of ethanol formation from syngas between the stepped Rh(211) and the flat Rh(111) surfaces have been compared to examine the effect of surface structure on catalytic performance. Furthermore, the promoter Mn-promoted MnRh(211) surface is employed to investigated the effect of surface composition on catalytic performance. Our results show that on the Rh(211) surface, the most favorable route of ethanol formation is CO + 3H → CHO + 2H → CH_2O + H → CH_3 + O first produces CH_3, then CHO is inserted into CH_3 to CH_3CHO. Finally, ethanol is formed via the route of CH_3CHO + 2H → CH_3CH_2O + H→ C_2H_5OH; during the overall conversion process, CH_3 formation is much easier than CH_3OH formation; that is, Rh(211) can boost the CH_3 source contributing to the formation of C_2 oxygenates. However, starting from CH_3 species, CH_3CHO formation is energetically compatible with CH_4 formation, which reduces the productivity and selectivity of C_2 oxygenates. As a result, to achieve high productivity and selectivity of ethanol, Rh catalyst has to get help from other promoters and/or supports, by which CH_4 formation should be minimized and/or C_2 oxygenate formation from C_1 oxygenates should be maximized.

Compared to the flat Rh(111) surface, the stepped Rh(211) surface not only leads to the new formation pathway of CH_3 species and C_2 oxygenates but also boosts the formations of CH_3 species and C_2 oxygenates, which means that the productivity and selectivity of ethanol from syngas on the stepped Rh(211) surface can be improved. In addition, starting from C_2 oxygenates, on the flat Rh(111), ethanol is formed via the route of CH_3CO + 3H → CH_3COH + 2H → CH_3CHOH + H → C_2H_5OH; however, on the stepped Rh(211), ethanol is formed via the route of CH_3CHO + 2H → CH_3CH_2O + H → C_2H_5OH. Thus, surface structure can affect the catalytic performance of ethanol formation from syngas. In other words, the presence of stepped defects can result in a higher activity and selectivity to ethanol synthesis compared to the that of the flat Rh(111) surface.

When the promoter Mn is introduced into the Rh(211) surface, Mn can facilitate CHO insertion into CH_3 and CH_4 formation with a lower activation barrier compared to the pure Rh(211) surface; that is, the promoter Mn can increase the catalytic activity of MnRh(211). Meanwhile, CH_3CHO formation is much more favorable than CH_4 formation, both kinetically and thermodynamically, indicating that the Mn-promoted MnRh(211) surface exhibits a good selectivity to C_2 oxygenates rather than CH_4. As a result, the promoter Mn can significantly increase the activity and selectivity of C_2 oxygenate formation on the Rh catalyst, which agrees well with the reported experimental results.

AUTHOR INFORMATION

Corresponding Author

*No. 79 Yingze West Street, Taiyuan 030024, China. Tel.: +86 351 6018239. Fax: +86 351 6041237. E-mail: zhangriugang@tyut.edu.cn, zhangriguang1981@163.com.

Notes

The authors declare no competing financial interest.

ACKNOWLEDGMENTS

This work is financially supported by the National Natural Science Foundation of China (21276003, 21476155, and 21276171), the Natural Science Foundation of Shanxi Province (2014011012-2), and the Top Young Innovative Talents of Shanxi.

REFERENCES

(1) Gupta, M.; Smith, M. L.; Spivey, J. J. Heterogeneous Catalytic Conversion of Dry Syngas to Ethanol and Higher Alcohols on Cu-Based Catalysts. *ACS Catal.* **2011**, *1*, 641−656.

(2) Gong, J. L.; Yue, H. R.; Zhao, Y. J.; Zhao, S.; Zhao, L.; Lv, J.; Wang, S. P.; Ma, X. B. Synthesis of Ethanol via Syngas on Cu/SiO_2 Catalysts with Balanced Cu^0-Cu^+ Site. *J. Am. Chem. Soc.* **2012**, *134*, 13922−13925.

(3) Zhang, R. G.; Wang, G. R.; Wang, B. J. Insights into the Mechanism of Ethanol Formation from Syngas on Cu and an Expanded Prediction of Improved Cu-based Catalyst. *J. Catal.* **2013**, *305*, 238−255.

(4) Choi, Y. M.; Liu, P. Mechanism of Ethanol Synthesis from Syngas on Rh(111). *J. Am. Chem. Soc.* **2009**, *131*, 13054−13061.

(5) Mei, D. H.; Rousseau, R.; Kathmann, S. M.; Glezakou, V. A.; Engelhard, M. H.; Jiang, W. L.; Wang, C. M.; Gerber, M. A.; White, J. F.; Stevens, D. J. Ethanol Synthesis from Syngas over Rh-based/SiO_2 Catalysts: A Combined Experimental and Theoretical Modeling Study. *J. Catal.* **2010**, *271*, 325−342.

(6) Hu, J.; Wang, Y.; Cao, C.; Elliott, D. C.; Stevens, D. J.; White, J. F. Conversion of Biomass Derived Syngas to Alcohols and C_2 Oxygenates Using Supported Rh Catalysts in a Microchannel Reactor. *Catal. Today* **2007**, *120*, 90−95.

(7) Fang, K. G.; Li, D. B.; Lin, M. G.; Xiang, M. L.; Wei, W.; Sun, Y. H. A Short Review of Heterogeneous Catalytic Process for Mixed Alcohols Synthesis via Syngas. *Catal. Today* **2009**, *147*, 133−138.

(8) Mo, X. H.; Gao, J.; Umnajkaseam, N.; Goodwin, J. G., Jr. La, V, and Fe Promotion of Rh/SiO_2 for CO Hydrogenation: Effect on Adsorption and Reaction. *J. Catal.* **2009**, *267*, 167−176.

(9) Subramani, V.; Gangwal, S. K. A Review of Recent Literature to Search for an Efficient Catalytic Process for the Conversion of Syngas to Ethanol. *Energy Fuels* **2008**, *22*, 814−839.

(10) Spivey, J. J.; Egbebi, A. Heterogeneous Catalytic Synthesis of Ethanol from Biomass-Derived Syngas. *Chem. Soc. Rev.* **2007**, *36*, 1514−1528.

(11) Haider, M. A.; Gogate, M. R.; Davis, R. J. Fe-Promotion of Supported Rh Catalysts for Direct Conversion of Syngas to Ethanol. *J. Catal.* **2009**, *261*, 9−16.

(12) Subramanian, N. D.; Gao, J.; Mo, X. H.; Goodwin, J. G., Jr; Torres, W.; Spivey, J. J. La and/or V Oxide Promoted Rh/SiO_2 Catalysts: Effect of Temperature, H_2/CO Ratio, Space Velocity, and Pressure on Ethanol Selectivity from Syngas. *J. Catal.* **2010**, *272*, 204−209.

(13) Ngo, H.; Liu, Y. Y.; Murata, K. Effect of Secondary Additives (Li, Mn) in Fe-Promoted Rh/TiO_2 Catalysts for the Synthesis of Ethanol from Syngas. *React. Kinet., Mech. Catal.* **2011**, *102*, 425−435.

(14) Han, L. P.; Mao, D. S.; Yu, J.; Guo, Q. S.; Lu, G. Z. Synthesis of C_2-Oxygenates from Syngas over Rh-Based Catalyst Supported on SiO_2, TiO_2 and SiO_2-TiO_2 Mixed Oxide. *Catal. Commun.* **2012**, *23*, 20−24.

(15) Fan, Z. L.; Chen, W.; Pan, X. L.; Bao, X. H. Catalytic Conversion of Syngas into C_2 Oxygenates over Rh-Based Catalysts—Effect of Carbon Supports. *Catal. Today* **2009**, *147*, 86−93.

(16) He, J.; Zhang, W. N. Research on Ethanol Synthesis from Syngas. *J. Zhejiang Univ., Sci., A* **2008**, *9*, 714−719.

(17) Zhang, J.; Cao, X. M.; Hu, P.; Zhong, Z. Y.; Borgna, A.; Wu, P. Density Functional Theory Studies of Ethanol Decomposition on Rh(211). *J. Phys. Chem. C* **2011**, *115*, 22429−22437.

(18) Xu, Y.; Mavrikakis, M. Adsorption and Dissociation of O_2 on Gold Surfaces: Effect of Steps and Strain. *J. Phys. Chem. B* **2003**, *107*, 9298−9307.
(19) Mavrikakis, M.; Bäumer, M.; Freund, H. J.; Nørskov, J. K. Structure Sensitivity of CO Dissociation on Rh Surfaces. *Catal. Lett.* **2002**, *81*, 153−156.
(20) Olsson, L.; Zhdanov, V. P.; Kasemo, B. Role of Steps in the NO−CO Reaction on the (111) Surface of Noble Metals. *Surf. Sci.* **2003**, *529*, 338−348.
(21) Pedersen, F. A.; Greeley, J.; Norskov, J. K. Understanding of the Effect of Steps, Strain, Poisons, and Alloying: Methane Activation on Ni Surfaces. *Catal. Lett.* **2005**, *105*, 9−13.
(22) McAllister, B.; Hu, P. A Density Functional Theory Study of Sulfur Poisoning. *J. Chem. Phys.* **2005**, *122*, 084709−1−084709−6.
(23) Liu, Z. P.; Hu, P. General Rules for Predictiong Where a Catalytic Reaction Should Occur on Metal Surfaces: A Density Functional Theory Study of C−H and C−O Bond Breaking/Making on Flat, Stepped, and Kinked Metal Surfaces. *J. Am. Chem. Soc.* **2003**, *125*, 1958−1967.
(24) Hammer, B. The NO+CO Reaction Catalyzed by Flat, Stepped, and Edged Pd Surfaces. *J. Catal.* **2001**, *199*, 171−176.
(25) Kapur, N.; Hyun, J.; Shan, B.; Nicholas, J. B.; Cho, K. Ab Initio Study of CO Hydrogenation to Oxygenates on Reduced Rh Terraces and Stepped Surfaces. *J. Phys. Chem. C* **2010**, *114*, 10171−10182.
(26) Bhattacharjee, T.; Inderwildi, O. R.; Jenkins, S. J.; Riedel, U.; Warnatz, J. Oxidation of Hydrocarbons at Surface Defects: Unprecedented Confirmation of the Oxomethylidyne Pathway on a Stepped Rh Surface. *J. Phys. Chem. C* **2008**, *112*, 8751−8753.
(27) González, S.; Loffreda, D.; Sautet, P.; Illas, F. Theoretical Study of NO Dissociation on Stepped Rh(221) and RhCu(221) Surfaces. *J. Phys. Chem. C* **2007**, *111*, 11376−11383.
(28) Catapan, R. C.; Oliveira, A. A. M.; Chen, Y.; Vlachos, D. G. DFT Study of the Water−Gas Shift Reaction and Coke Formation on Ni(111) and Ni(211) Surfaces. *J. Phys. Chem. C* **2012**, *116*, 20281−20291.
(29) Behrens, M.; Studt, F.; Kasatkin, I.; Kühl, S.; Hävecker, M.; Abild-Pedersen, F.; Zander, S.; Girgsdies, F.; Kurr, P.; Kniep, B. L.; Tovar, M.; Fischer, R. W.; Nørskov, J. K.; Schlögl, R. The Active Site of Methanol Synthesis over $Cu/ZnO/Al_2O_3$ Industrial Catalysts. *Science* **2012**, *336*, 893−897.
(30) Ojeda, M.; Granados, M. L.; Rojas, S.; Terreros, P.; García-García, F. J.; Fierro, J. L. G. Manganese-Promoted Rh/Al_2O_3 for C_2-Oxygenates Synthesis from Syngas Effect of Manganese Loading. *Appl. Catal., A* **2004**, *261*, 47−55.
(31) Ma, H. T.; Yuan, Z. Y.; Wang, Y.; Bao, X. H. Temperature-Programmed Surface Reaction Study on C_2-Oxygenate Synthesis over SiO_2 and Nanoporous Zeolite Material Supported Rh-Mn Catalysts. *Surf. Interface Anal.* **2001**, *32*, 224−227.
(32) de Jong, K. P.; Glezer, J. H. E.; Kuipers, H. P. C. E.; Knoester, A.; Emeis, C. A. Highly Dispersed Rh/SiO_2 and $Rh/MnO/SiO_2$ Catalysts: 1. Synthesis, Characterization, and CO Hydrogenation Activity. *J. Catal.* **1990**, *124*, 520−529.
(33) van der Berg, F. G. A.; Glezer, J. H. E.; Sachtler, W. M. H. The Role of Promoters in CO/H_2 Reactions: Effects of MnO and MoO_2 in Silica Supported Rhodium Catalysts. *J. Catal.* **1985**, *93*, 340−352.
(34) Li, F. Y.; Jiang, D. E.; Zeng, X. C.; Chen, Z. F. Mn Monolayer Modified Rh for Syngas-to-Ethaol Conversion: A First-Principles Study. *Nanoscale* **2012**, *4*, 1123−1129.
(35) Treviño, H.; Sachtler, W. M. H. On the Nature of Catalyst Promotion by Manganese in CO Hydrogenation to Oxygenates over RhMn/NaY. *Catal. Lett.* **1994**, *27*, 251−258.
(36) Zhao, Y. H.; Yang, M. M.; Sun, D. P.; Su, H. Y.; Sun, K. J.; Ma, X. F.; Bao, X. H.; Li, W. X. Rh-Decorated Cu Alloy Catalyst for Improved C_2 Oxygenate Formation from Syngas. *J. Phys. Chem. C* **2011**, *115*, 18247−18256.
(37) Chen, G. C.; Guo, C. Y.; Huang, Z. J.; Yuan, G. Q. Synthesis of Ethanol from Syngas over Iron-Promoted Rh Immobilized on Modified SBA-15 Molecular Sieve: Effect of Iron Loading. *Chem. Eng. Res. Des.* **2011**, *89*, 249−253.
(38) Ito, S. I.; Ishiguro, S.; Nagashima, K.; Kunimori, K. CO Hydrogenation over a $RhVO_4/SiO_2$ Catalyst after H_2 Reduction. *Catal. Lett.* **1998**, *55*, 197−199.
(39) Luo, H. Y.; Zhang, W.; Zhou, H. W.; Huang, S. Y.; Lin, P. Z.; Ding, Y. J.; Lin, L. W. A Study of Rh-Sm-V/SiO_2 Catalysts for the Preparation of C_2-Oxygenates from Syngas. *Appl. Catal., A* **2001**, *214*, 161−166.
(40) Zamvelli, T.; Wintterlin, J.; Throst, J.; Ertl, G. Identification of the "Active Sites" of a Surface-Catalyzed Reaction. *Science* **1996**, *273*, 1688−1690.
(41) Kresse, G.; Hafner, J. Ab Initio Molecular Dynamics for Liquid Metals. *Phys. Rev. B: Condens. Matter Mater. Phys.* **1993**, *47*, 558−561.
(42) Kresse, G.; Furthmuller, J. Efficient Iterative Schemes for Ab Initio Total-Energy Calculations Using a Plane-Wave Basis Set. *Phys. Rev. B: Condens. Matter Mater. Phys.* **1996**, *54*, 11169−11186.
(43) Kresse, G.; Furthmuller, J. Efficiency of Ab-Initio Total Energy Calculations for Metals and Semiconductors Using a Plane-Wave Basis Set. *Comput. Mater. Sci.* **1996**, *6*, 15−50.
(44) Perdew, J. P.; Chevary, J. A.; Vosko, S. H.; Jackson, K. A.; Pederson, M. R.; Singh, D. J.; Fiolhais, C. Atoms, Molecules, Solids, and Surfaces: Applications of the Generalized Gradient Approximation for Exchange and Correlation. *Phys. Rev. B: Condens. Matter Mater. Phys.* **1992**, *46*, 6671−6687.
(45) Kresse, G.; Joubert, D. From Ultrasoft Pseudopotentials to the Projector Augmented-Wave Method. *Phys. Rev. B: Condens. Matter Mater. Phys.* **1999**, *59*, 1758−1775.
(46) Monkhorst, H. J.; Pack, J. D. Special Points for Brillouin-Zone Integrations. *Phys. Rev. B: Condens. Matter Mater. Phys.* **1976**, *13*, 5188−5192.
(47) Methfessel, M.; Paxton, A. T. High-Precision Sampling for Brillouin-Zone Integration in Metals. *Phys. Rev. B: Condens. Matter Mater. Phys.* **1989**, *40*, 3616−3621.
(48) Sheppard, D.; Xiao, P.; Chemelewski, W.; Johnson, D. D.; Henkelman, G. A Generalized Solid-State Nudged Elastic Band Method. *J. Chem. Phys.* **2012**, *136*, 074103−1−8.
(49) Sheppard, D.; Terrell, R.; Henkelman, G. Optimization Methods for Finding Minimum Energy Paths. *J. Chem. Phys.* **2008**, *128*, 134106−1−10.
(50) Henkelman, G.; Jónsson, H. A Dimer Method for Finding Saddle Points on High Dimensional Potential Surfaces Suing only First Derivatives. *J. Chem. Phys.* **1999**, *111*, 7010−7022.
(51) Olsen, R. A.; Kroes, G. J.; Henkelman, G.; Arnaldsson, A.; Jónsson, H. Comparison of Methods for Finding Saddle Points Without Knowledge of the Final States. *J. Chem. Phys.* **2004**, *121*, 9776−9792.
(52) Kiennemann, A.; Breault, R.; Hindermann, J. P.; Laurin, M. Ethanol Promotion by the Addition of Cerium to Rhodium-Silica Catalysis. *J. Chem. Soc., Faraday Trans. 1* **1987**, *83*, 2119−2128.
(53) Zhao, Y. H.; Sun, K. J.; Ma, X. F.; Liu, J. X.; Sun, D. P.; Su, H. Y.; Li, W. X. Carbon Chain Growth by Formyl Insertion on Rhodium and Cobalt Catalysts in Syngas Conversion. *Angew. Chem., Int. Ed.* **2011**, *50*, 5335−5338.
(54) Stroppa, A.; Mittendorfer, F.; Andersen, J. N.; Parteder, G.; Allegretti, F.; Srunev, S.; Netzer, E. P. Adsorption and Dissociation of CO on Bare and Ni-Decorated Stepped Rh(553) Surfaces. *J. Phys. Chem. C* **2009**, *113*, 942−949.
(55) Luo, H. Y.; Lin, P. Z.; Xie, S. B.; Zhou, H. W.; Xu, C. H.; Huang, S. Y.; Lin, L. W.; Liang, D. B.; Yin, P. L.; Xin, Q. The Role of Mn and Li Promoters in Supported Rhodium Catalysts in the Formation of Acetic Acid and Acetaldehyde. *J. Mol. Catal. A: Chem.* **1997**, *122*, 115−123.